

## Pointing the ATA Dishes

G. R. Harp, M. C. Fleming, R. A. Ackermann, D. R. DeBoer, and G. C. Bower

### Abstract

This memo discusses the results of radio and optical pointing measurements on the ATA antennas. Using the “Room Temperature Cryo” version of the ATA feed, we demonstrate that the pointing specification of the ATA is met with existing hardware. Radio measurements, characterizing the longer-term effects, are made at a relatively low frequency (2.5 GHz) where the pointing specification (120 arc seconds RMS) is only 2% of the primary beam FWHM. Measurements of the sun with the derived pointing model in place yields an RMS of 88" over a 4.7 hour track (1.75% of the FWHM primary beam). Currently, the sensitivity of the receiver and the frequency range of the prototype downconverter currently limit our ability to measure the intrinsic pointing errors. Future measurements at higher frequencies and with greater sensitivity should demonstrate pointing accuracies exceeding the specification even further. Optical pointing tests to characterize the tracking on short time scales show that the tracking is smooth and short time scale deviations are less than 30" RMS.

### Introduction

The quantitative basis for the ATA pointing specification is found by examining the ways we intend to use it. For example, when forming a beam on a known point source (such as a SETI target or a pulsar) only modest pointing accuracy is required. A random distribution of pointing errors with RMS = 30% of the primary beam FWHM (full-width at half-maximum) will degrade the synthetic beam power by less than 10%, and this might be considered adequate for such observations.

The most stringent pointing accuracy is required for large angle image mosaics, as in the HI survey. We wish to overlap sub-images (or “tiles”) of a larger “mosiaced” image where each tile is acquired with a different pointing. In cases where a strong source (like Cas A) is present on the edge of a tile, the contribution from that source varies strongly with only small changes in pointing. Good image fidelity is achieved only when the contribution of edge sources is known with high accuracy. Hence the pointing spec is set to 120" at the ATA, which represents approximately 10% of the primary beam FWHM at the highest observation frequency (11.2 GHz), and just over 1% of the primary beam at the HI frequency. Note that this specification is for situations with no wind. It increases to twice that value at 15 mph winds, with no formal specification for winds exceeding 15 mph.

To formally prove the pointing spec at the ATA, a specific milestone has been set: “Acquire and track a source with an RMS pointing error of 120" or less, for a period of not less than two hours, at wind velocities not to exceed 15 mph.” In this document we demonstrate that this goal has been achieved and describe the mathematical pointing model that was used to attain this result. Radio observations are made with the “Room

Temperature Cryo” (RTC) version of the ATA feed placed on Antenna 1. This engineering development feed is electrically identical to the ones to be used in the final system, but has no internal low noise amplifier. As a result the sensitivity is relatively low, so observations are performed on L-band satellites and the sun, which are the only moving objects whose signal is strong enough to make effective single-dish measurements with the current system. Similar studies using RPA feeds on Antennas 2 and 3 show comparable results.

To augment these results, a telescopic video camera was attached to Antenna 3 and used to track planets and stars. These data show that the tracking is smooth on short time scales, and that the RMS deviations in the optical data are less than 30”.

## Pointing Model

Each ATA dish is equipped with two encoders that give readings of the nominal azimuth and elevation angles with 22 arc second resolution.<sup>1</sup> If the dish were perfect, these readings could be used directly to execute blind pointing. But slight mechanical misalignments cause the dish to point to a place different from the encoder readings, and these differences may vary from dish to dish. The differences are small, so there is a 1:1 mapping between encoder readings and actual position on the sky.<sup>2</sup> We represent this mapping with a “pointing model.”

Telescope pointing models have been well studied in the past, and commercial packages are available to simplify the process. We have chosen to use the TPOINT pointing software package developed by Patrick Wallace. This package is unquestionably adequate, as evidenced by the fact that it has been adopted for the Atacama Large Millimeter Array whose pointing requirements are 100 times more stringent than our own.

TPOINT starts with a (generalized) physical model of an Az-El telescope and describes most pointing corrections in terms of mechanical factors. For example, the azimuthal axis might be tilted with respect to zenith, or the receiver might be displaced from its nominal position. After the largest errors are modeled in this way, the user may add polynomial or sinusoidal pointing corrections describing any dependence of azimuth errors on azimuth, elevation errors on elevation, and/or cross terms. We gratefully acknowledge consultations with Dr. Wallace, who helped us develop a preliminary pointing model with the following terms:

IA = Azimuthal Encoder Offset

IE = Elevation Encoder Offset

HASA2 = Az correction  $\propto \sin^2(\text{Az})$

HACA2 = Az correction  $\propto \cos^2(\text{Az})$

---

<sup>1</sup> By resolution, we mean the distance between encoder steps. These encoders are being used only for the prototyping stage. In the final ATA array, we intend to use encoders with 9” step size.

<sup>2</sup> Except very close to zenith. If there is a collimation error or if the azimuth and elevation axes are not perpendicular, then there may be a small region near zenith that is unreachable. This region is typically smaller than the keyhole (the region directly overhead where a source can not be tracked with an az-el mount), so irrelevant in most cases.

HACE = Az correction  $\propto \cos(\text{El})$

TF = Tube Flexure – El correction to compensate Hooke's Law bending of structure

CA = Receiver offset affecting azimuth collimation (in elevation this is absorbed by IE)

AN = Tipping of Az axis toward North

AW = Tipping of Az axis toward West

Following the advice of Dr. Wallace, we intend to replace the HACE term with HSSE (Az correction  $\propto \tan(\text{El})$ ) in the next iteration, since this is physically more meaningful (approximates non-perpendicularity of Az and El axes). The equations for implementing these terms are well documented in the TPOINT software manual.

## GPS Observations

We bootstrap the pointing model by observing radio satellites at L-band and S-band. A very crude pointing model having only Az and El offsets is first determined by peaking the radio signal from one or two geostationary satellites. Next a computer program executes a systematic search for GPS satellites. This program loops over all the GPS satellites, and seeks out in turn each of those that are currently above the dish horizon (eventually  $15^\circ$  elevation, but about  $20^\circ$  at present). The dish executes a 10-point cross centered on the (moving) GPS satellite (Fig. 1). The scale in Fig. 1 is in units of the expected primary beam HWHM (half-width at half maximum), which in the case of GPS is  $1.11^\circ$ .

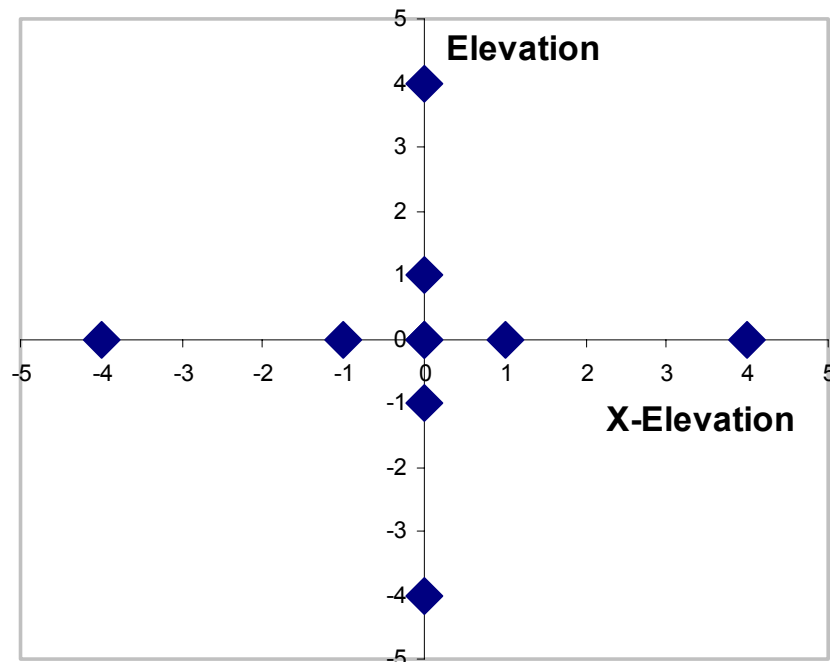


Figure 1: Relative positions of the 10-point cross pattern used to sample the GPS satellite position. The central position is measured twice. Units are HWHM of the primary beam pattern.

The ATA “Software” Correlator is used to accumulate data at each position for 5 seconds<sup>3</sup>. The total power in one polarization is accumulated at each point. For each linear array of points, the two outer points are used to determine an assumed constant background value, and then the inner three points are fit with a Gaussian beam profile. Deviations of the Gaussian centroid from the zero-offset position are recorded as a “pointing error” which is used to a) determine the pointing model coefficients and b) subsequently check the performance of the pointing model.

The 10-point pattern and Gaussian fit is repeated 4 times on each satellite, and then the program moves on to the next satellite in the list. When the end of the list is reached, the program starts over at the beginning of the list.

Figure 2 summarizes 35 hours of pointing data accumulated on GPS satellites with ATA Antenna 1 (vertical polarization – note that GPS satellites transmit right-handed circularly polarized radiation). This plot was generated by TPOINT, and displays 450 measurements (symbols) and their associated errors (scaled lines) on a spherical projection of the sky’s hemisphere (zenith at center). Because GPS satellites do not pass directly over the North Pole, no observations are made over a substantial region towards the north. Apart from this region, however, the satellites give a reasonably uniform sampling of pointing position.

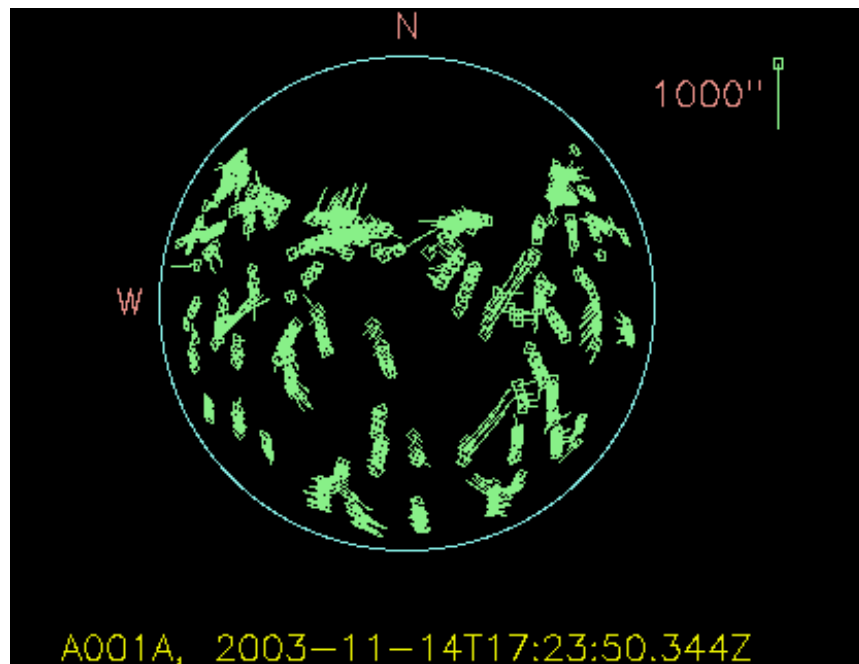


Figure 2: Spherical projection of 35 hours of continuous GPS observations made with Antenna 1. The UTC date at the bottom indicates the start time of the data set.

<sup>3</sup> The full correlator bandwidth is 20 MHz and its throughput is ~1% of the data stream. A mask with a 2 MHz “window” is centered on the nominal GPS transmission frequency (1.5754 GHz). Note that GPS generates a spread-spectrum signal where most of the GPS power is spread over a 1 MHz bandwidth.

Using these data, a first-pass pointing model is generated. Figure 3 shows the residual pointing errors in elevation (vertical) and cross-elevation (horizontal) with *ex post facto* application of the pointing model. The inner circle on the plot indicates 370" RMS residual error which is a promising first attempt.

In this example, the data appear to follow a bimodal distribution. At the center is a tight group of points surrounded by a half-dozen episodes (groups of 4) showing a much broader residual distribution. Preliminary analysis suggests that the outlier episodes are associated with early morning observations (i.e. sunrise). Further observations with more accurate time-tagging are underway to study this phenomenon. Notice that in the daytime observations presented below, such outlier events do not appear.

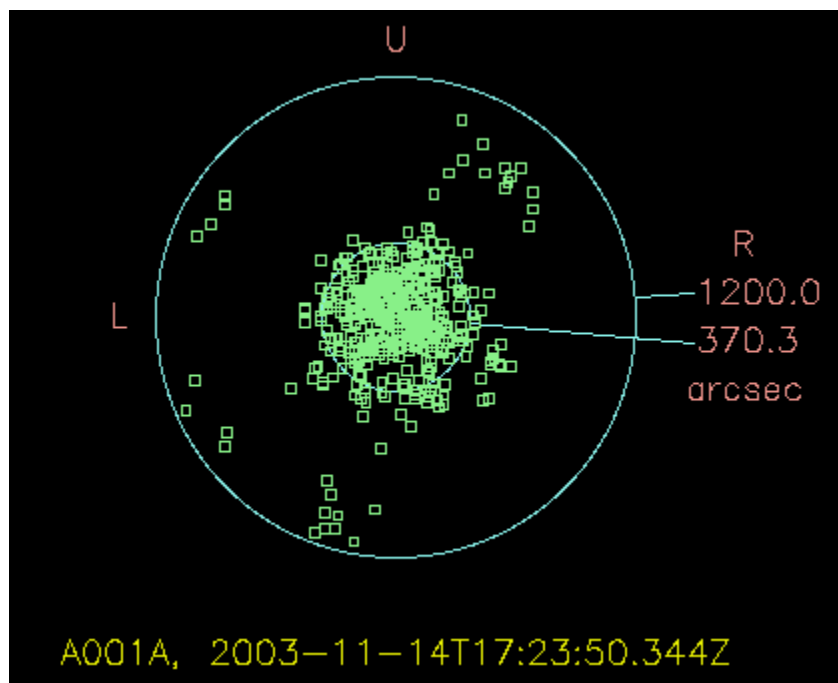


Figure 3: Distribution of residual pointing errors following application of our pointing model to the data in Fig. 2. Vertical displacements indicate elevation error, while horizontal displacements indicate cross-elevation error.

If we neglect the outlier episodes (for the moment) then the remaining points at the center have a tighter distribution with an RMS error  $\sim 250''$ . We can show that this distribution is dominated by random errors (i.e. noise) by looking at the statistics of the 4-point groups. Within each 4-point group we subtract the average residual pointing error and examine the distribution of errors that remain. Since each group samples a small region of the sky, this analysis approximates the action of a perfect pointing model. Following this

procedure on *all* of the data, the residual RMS pointing error is  $200''$ ,<sup>4</sup> which represents our estimate of the noise. This is only 2.5% of the primary beam FWHM.

One kind of systematic error that is not accounted for by a mathematical pointing model is hysteresis. With hysteresis, the observed satellite position is dependant on the position of the previous measurement. Fortunately, TPOINT has a built-in analysis tool to look for hysteresis and quantify it. Each data point in Fig. 4 has angular position and radius proportional to the direction and distance it moved just prior to making that observation. The lines indicate the residual pointing error. If the dish had substantial hysteresis then the lines might exhibit some pattern, such as being splayed radially inward.

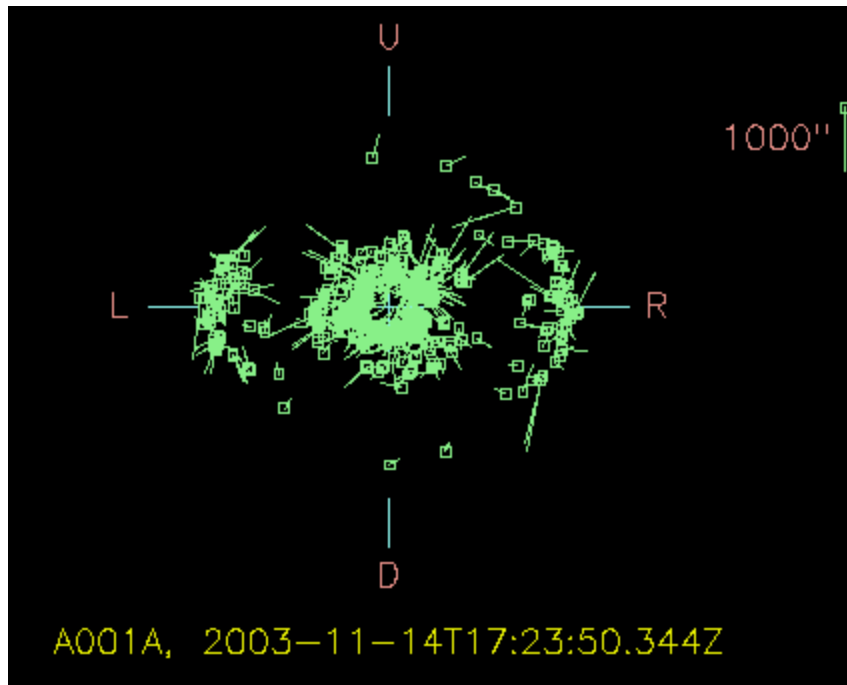


Figure 4: Hysteresis plot for the data in Fig. 2. From this plot we estimate the average hysteresis at  $20''$  which is comparable to the encoder step size.

A numerical analysis of the data in Fig. 4 indicates an average hysteresis of  $20''$ . This is almost the same as the encoder step size,  $22''$ , which is the only known source of hysteresis. Such agreement is fortuitous, considering the noise level. This analysis makes the assumption that the hysteresis comes from large-scale movements between observations and is unaffected by small-scale adjustments during acquisition.<sup>5</sup> Hence we should revisit the hysteresis issue at a later date if the “random” errors at high frequencies appear to be out of proportion.

<sup>4</sup> By subtracting the average residual error, we are simulating a pointing model with more than 100 degrees of freedom, many more than would be used in practice. As a result, our estimate of the errors due to noise alone may be low. Notice that in calculating the RMS, we have normalized properly to take account for the pointing model degrees of freedom.

<sup>5</sup> P.T. Wallace, “A Telescope Pointing Analysis System,” (TPOINT manual), Feb. 11, 2003, p. 47.

As a final point, we note that similar GPS observations have been made on both antennas 2 and 3 (A2 and A3), which employ RPA feeds. These feeds have about the same sensitivity as the RTC feed on A1, but they have a smaller bandwidth (1-3 GHz). We have constructed first-order pointing models for these antennas, and the coefficient values are on the same order of magnitude as those for A1.

## **Solar Observations**

To further improve the pointing model, we make observations at a higher frequency where the primary beam width is smaller. The conventional way to do this is to use celestial sources, which are typically broadband. Unfortunately the system temperature at the time of these measurements was quite high, perhaps 1000 K at L-band, which precluded effective measurement of most celestial sources until the cryogenic feed is installed. The only natural source we can observe is the sun.

Recently, a dual-path high frequency downconverter (on loan from SETI Institute) was installed which will enable solar observations up to  $\sim 10$  GHz. However, all the measurements described here were made with the RPA downconverter, which operates over the frequency range 0.5-2.5 GHz. Thus our minimum primary beam FWHM is  $1.4^\circ$ . Solar observations are made with correlator settings similar to those used for GPS: center frequency 2.5 GHz, bandwidth = 2 MHz, observation time = 5 sec and duty cycle = 1%.

The GPS pointing model described above was refined by fitting additional GPS measurements and solar observations taken over several days. Because of the smaller primary beam width, the solar measurements have substantially less scatter. Finally, the pointing model was fixed and the sun was observed again.

The results of one such run are shown in Fig. 5. Here we tracked the Sun continuously from rise to set (within antenna limits) on one day. Over this period (4.7 hours) about 100 measurements were obtained. The RMS residual error is  $88''$ , substantially below the pointing specification of  $120''$ .

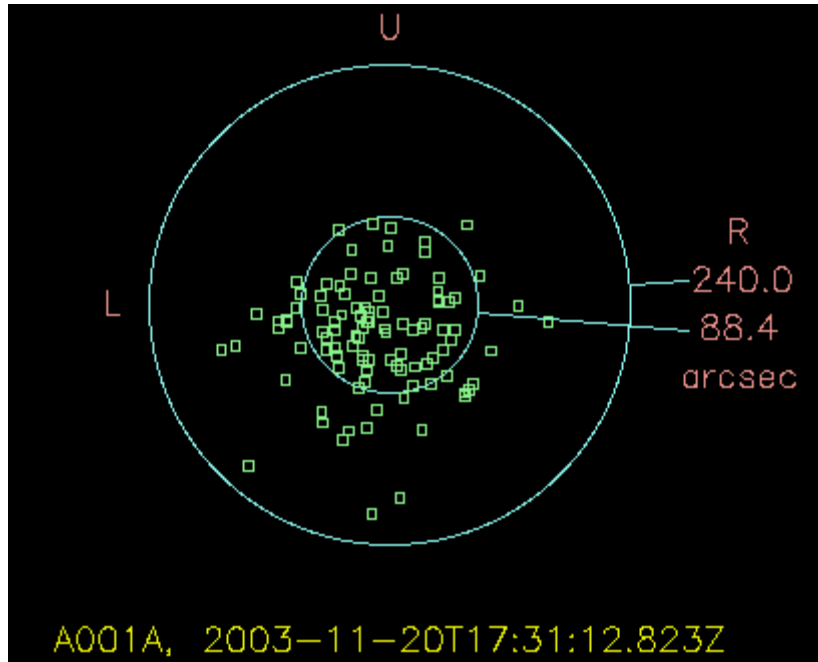


Figure 5: Scatter plot of the residuals from solar observations acquired over a 4.7 hour period on the indicated date. The RMS deviation is  $88''$ , and exceeds the ATA pointing specification.

With the current pointing model there is a detectable offset of the residual errors towards the lower left hand corner of the plot. This suggests that the pointing model could be further improved, leading to an even better result. At this frequency, however, the random variations due to noise are the dominant source of residual error. Similar results were obtained with an RPA feed on antenna 3.

## Optical Pointing Tests

The results of the previous section demonstrate the successful implementation of a pointing model exceeding the pointing goal, however the radio pointing data were acquired with 5 s integration at each point which could mask high frequency dish motions. To validate the pointing on short time scales we attached a video camera to one antenna and used it to track bright stars. Such optical testing is precise and rapid, as high resolution images are acquired with only 0.03 s integration time. Optical pointing suffers from the complication that the optical and radio detectors may be misaligned. But even without perfect alignment optical testing provides a sensitive probe of high frequency jitter in the tracking.<sup>6</sup>

We attached a commercial color CCD camera to the secondary reflector on A3. This is a high quality Canon VCC4 camera with pan/tilt motion stage, 1-16 $\times$  variable zoom, manual/auto focus, manual/auto expose, and approximately  $400 \times 300 \times 3$  color CCD.

<sup>6</sup> More specifically, the radio measurements demonstrate the success of the pointing model over the sky, and quantify the thermal effects; while the optical measurements quantify the short-term rigidity of the mount, and of the primary and secondary positions (since the camera was mounted on the secondary, which was connected to the primary).

Further telescopic magnification is achieved with a fixed 2× zoom lens. The camera is held in a commercial temperature controlled enclosure with plastic radome. The camera output is NTSC which is converted to digital using a TV capture card on a small computer mounted beside the camera. Images are captured at 640 × 480 resolution and with maximal magnification, one pixel in the final image represents 16". Because the camera is cantilevered on the front of the secondary, it is probably more sensitive to vibrations in the antenna than the radio receiver, if any such occur. For these initial studies we chose Mars for an optical target, but we have seen other celestial objects such as Pollux (a magnitude 1 star).



Figure 6: Image of Mars acquired with the VCC4 camera. This is a blow-up of the center area of the larger image.

Figure 6 shows a blow up of the central 12% of Mars' image. The full width of the image is about 1200". This is to demonstrate the nature of the camera, where the image is better resolved perpendicular to the NTSC scan line than parallel to it. A better perception of the image quality may be obtained by examining a short movie of Mars tracking which can be found at:

<http://astron.berkeley.edu/~gharp/Mars.mov>

OR

<http://astron.berkeley.edu/~gharp/Mars.gif>

This movie was taken over a four-minute period but plays back at a faster rate.

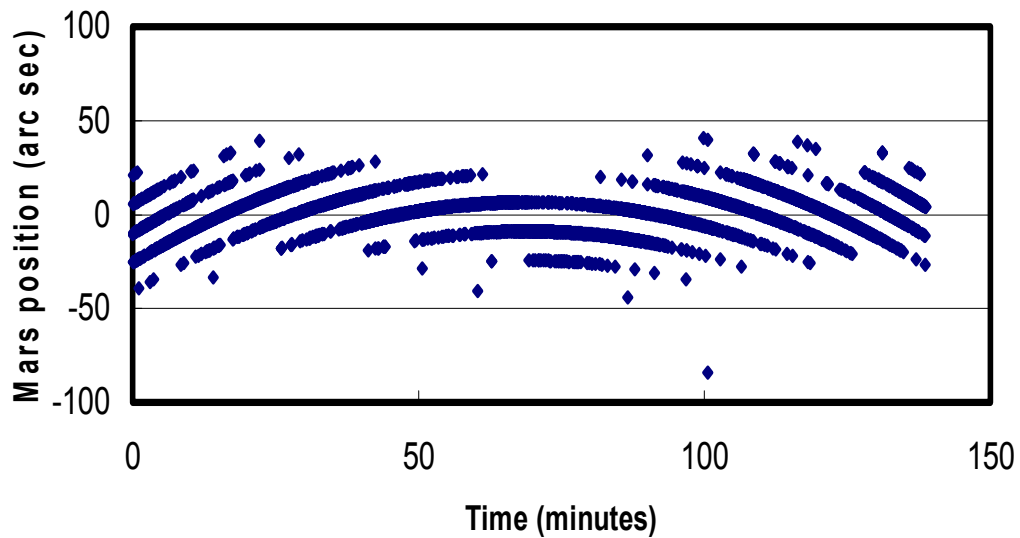


Figure 7: Vertical variation of Mars image in the optical camera as a function of time. Long-term drifts due to collimation offsets have been removed.

Figures 7 and 8 show results from a two hour track of Mars with our system. The 30 Hz image stream was sampled at 0.5 Hz. The position of the pixel with maximum value is taken as the measured position of Mars. The angular scale in the image was calibrated by rotating the camera by  $0.5^\circ$  and observing the image shift. The striped appearance is due to the finite pixel size coupled with the simple “brightest” pixel pointing definition.

Mars’ image was observed to drift slowly as a function of time, moving  $\sim 1000''$  between transit and set. We believe the major contributor to this shift is the collimation error between the optical and radio axes, which could easily be a degree. Since we are mainly interested in short time scale effects, Mars’ vertical and horizontal position as a function of time were fit with quadratic polynomials, simulating an *ex post facto* pointing model. These polynomials were subtracted from the data to give the results plotted in Figs. 7 and 8.

After polynomial subtraction, the residual pointing errors are small, with a radial RMS displacement of  $25''$ . This gives quantitative backing to the impression one gets from the movie: that the antenna tracking is smooth and steady. The granularity in Figs. 7 and 8 comes from pixellation in the image. The data in Fig. 8 have a larger random component than those in Fig. 7, which is consistent with the lateral broadening of the image in Fig. 6. Some nonrandom structure in Fig. 8 indicates that further pointing model refinement may be possible.

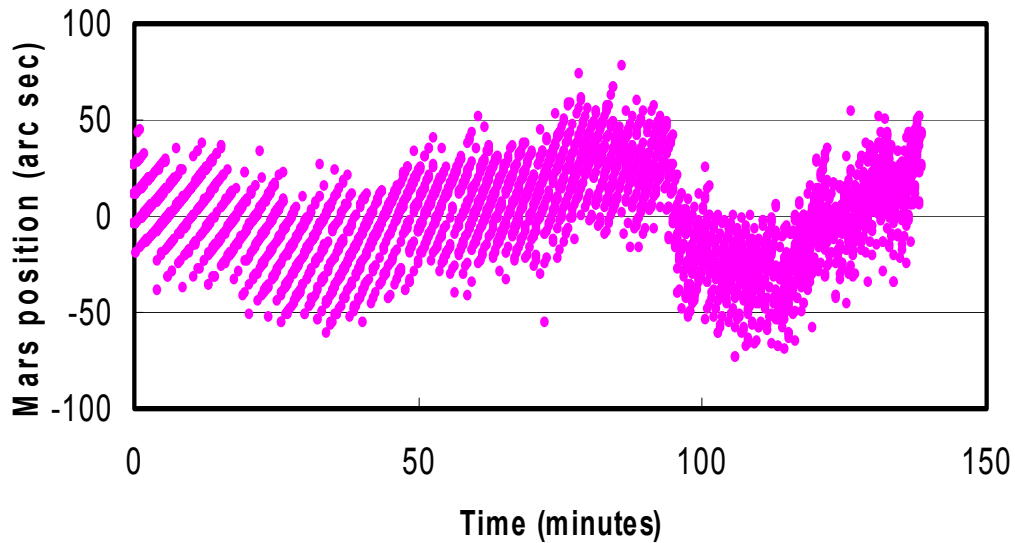


Figure 8: Horizontal variation of Mars image in the optical camera as a function of time, over the same time period as in Fig. 8. Long-term drifts due to collimation offsets have been removed.

## Conclusion

We have demonstrated that the ATA antenna hardware and control system achieve the telescope specification. The present memo focuses on initial results obtained with prototype receivers and a newly installed video camera. As the sensitivity and frequency bandwidth of the telescope improves, and as we gain experience, we expect that the pointing will even more significantly exceed the specification.

The ATA promises to be an exceptional instrument for large solid angle imaging surveys of the centimeter radio spectrum. In many cases, the image fidelity of such surveys is constrained by some exceptionally strong radio sources that confound measurements in their vicinity. The ATA's unique Gregorian design and clear aperture give rise to a well-behaved primary beam pattern. This beam pattern, in turn, makes it possible to accurately correct for confounding sources, but only if strict pointing conditions are met. The excellent pointing characteristics of the ATA antennas, as demonstrated here, bode well for the ATA's future survey capabilities.